research papers

CrossMark

Optimizing X-ray mirror thermal performance using matched profile cooling

Lin Zhang,[a,b]* Daniele Cocco,[a] Nicholas Kelez,[a] Daniel S. Morton,[a] Venkat Srinivasan[a] and Peter M. Stefan[a]

[a]LCLS, SLAC National Accelerator Laboratory, 2575 Sand Hill Road, Menlo Park, CA 94025, USA, and [b]ISDD, European Synchrotron Radiation Facility, 71 Avenue des Martyrs, Grenoble 38043, France. *Correspondence e-mail: zhanglin@slac.stanford.edu

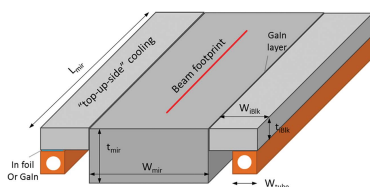To cover a large photon energy range, the length of an X-ray mirror is often longer than the beam footprint length for much of the applicable energy range. To limit thermal deformation of such a water-cooled X-ray mirror, a technique using side cooling with a cooled length shorter than the beam footprint length is proposed. This cooling length can be optimized by using finite-element analysis. For the Kirkpatrick–Baez (KB) mirrors at LCLS-II, the thermal deformation can be reduced by a factor of up to 30, compared with full-length cooling. Furthermore, a second, alternative technique, based on a similar principle is presented: using a long, single-length cooling block on each side of the mirror and adding electric heaters between the cooling blocks and the mirror substrate. The electric heaters consist of a number of cells, located along the mirror length. The total effective length of the electric heater can then be adjusted by choosing which cells to energize, using electric power supplies. The residual height error can be minimized to 0.02 nm RMS by using optimal heater parameters (length and power density). Compared with a case without heaters, this residual height error is reduced by a factor of up to 45. The residual height error in the LCLS-II KB mirrors, due to free-electron laser beam heat load, can be reduced by a factor of ~11 *below* the requirement. The proposed techniques are also effective in reducing thermal slope errors and are, therefore, applicable to white beam mirrors in synchrotron radiation beamlines.

1. Introduction

The Linac Coherent Light Source (LCLS) at the SLAC National Accelerator Laboratory, the world's first hard X-ray free-electron laser (FEL), produces ultrafast X-ray pulses of unprecedented brilliance. All six experimental stations are supporting user science and producing high-impact scientific results (Mankowsky *et al.*, 2014; Chapman *et al.*, 2011; Seibert *et al.*, 2011). In order to increase the capabilities and capacity of the LCLS, the Department of Energy has funded the LCLS-II project (Galayda, 2014; LCLS-II, 2013). In addition to the existing LCLS-I copper linac that delivers FEL pulses at 120 Hz, LCLS-II will use a 4 GeV superconducting (SC) linear accelerator to provide FEL pulses with high repetition rates, up to 1 MHz. Two lines of variable-gap undulators will be used for soft and hard X-ray beamlines. The LCLS-II light source, with high repetition rates, will enable a broad range of high-resolution, coherent 'pump probe' experiments over a large photon energy range, from 0.2 to 5 keV. The average power of the FEL beam from the SC linac will range from 20 to 200 W. In addition to the ultrashort pulse length, the FEL beam has a narrow energy bandwidth, down to less than 10^{-4}, thanks to self-seeding technology (Feldhaus *et al.*, 1997; Amann *et al.*,

2012; Cocco *et al.*, 2013; Ratner *et al.*, 2015) and small beam divergence. For the soft X-ray (SXR) beamline, the beam divergence decreases from 21 µrad to 4.4 µrad as the photon energy increases from 200 eV to 1300 eV.

X-ray optics for the SXR beamline includes a pair of flat distribution mirrors and a Kirkpatrick–Baez (KB) mirror system. To preserve the photon flux and wavefront, mirror height errors should be limited to as low as 1 nm RMS, while the mirrors absorb about 10% of the incident X-ray beam power. Because the baseline height error requirement already pushes the state-of-the-art for optic fabrication, the heat-load-induced mirror distortion must be minimized, to satisfy overall performance requirements.

Thermal deformation of X-ray optics for third-generation synchrotron light sources has been studied extensively, by both experiment and simulation. For monochromator silicon crystals, liquid nitrogen (LN_2) cooling has been widely investigated (Marot *et al.*, 1992; Zhang, 1993; Rogers *et al.*, 1995; Lee *et al.*, 1995, 2000, 2001; Zhang *et al.*, 2003, 2013*a*; Bilderback *et al.*, 2000; Mochizuki *et al.*, 2001) and subsequently used in many beamlines. The motivation to use LN_2 cooling for monochromator crystals is based on the following points. (1) The thermal deformation of X-ray optics is proportional to the ratio α/k, where α and k are the thermal expansion coefficient and the thermal conductivity, respectively, of the crystal material. The ratio α/k for silicon at LN_2 temperature (77 K at 1 atm) is much lower than that at room temperature. Therefore, LN_2 cooling can significantly reduce the thermal deformation of the silicon crystal, compared with water cooling at near room temperature. (2) The beam footprint on a monochromator crystal (X-ray beam illuminated area) is variable and typically much smaller than the crystal size, because of the large and variable Bragg angle. This approach can also be applied to high-heat-load mirrors with silicon substrates, but implementation of such LN_2 cooling is much more expensive than water cooling and presents additional complexity. Consequently, water cooling is the technique of choice for most white beam mirrors in third-generation synchrotron light sources. To minimize thermal deformation of a water-cooled mirror, one effective method is to cool the mirror along the 'top-up-sides'[1] of the substrate, fully illuminate – or overfill – the mirror length, use secondary slits downstream of the mirror to shape the beam to the desired final size, and optimize the mirror cross section with notches (Zhang, 2010; Zhang *et al.*, 2012, 2013*b*). The thermal slope error of such a mirror, with about 800 W of absorbed beam power, can be minimized to 0.018 µrad. This technique is widely used for white beam mirrors and most white or pink beam multilayer optics at the ESRF Upgrade beamlines. In contrast, RMS thermal slope errors in the case of mirror cooling on the

bottom face (opposite the mirror optical surface) can reach 200 µrad. A mirror cross section with notch structures has previously been proposed (Khounsary, 1999).

For the flat distribution mirrors and Kirkpatrick–Baez (KB) mirrors proposed for the LCLS-II SXR beamline, the beam footprint length on the mirror varies by a factor of 4.8, as the photon energy changes from 200 eV to 1300 eV, and can be much shorter than the mirror length. This partial mirror illumination compromises effectiveness of the mirror thermal deformation reduction technique mentioned above. With a beam footprint much shorter than the mirror length, thermal conduction induces temperature variation in the mirror meridional (tangential) direction. This variation creates a thermal bump component, which is not spherical and cannot be corrected using a mechanical bender. In this paper, we report a strategy to correct this bump effect, and minimize the thermal deformation. First, we present some key parameters of the KB mirror and a finite-element model of a rectangular mirror for thermal deformation minimization. Then, we focus on a mirror, water cooled on the top-up-sides, with variable cooling length. Finally, we propose a mirror water cooled on the full-length top-up-sides with variable-length and variable-power-density adjustable electric heaters.

2. Mirror description and modelling

2.1. Mirror description

X-ray optics in the LCLS-II SXR beamline includes two flat distribution mirrors and a KB mirror system. The latter consists of a set of two mirrors, oriented perpendicularly to each other. The KB mirror system is located about $d_0 = 105$ m from the undulator exit end, and focuses between 2 and 5 m downstream of the second mirror in the KB mirror system. These mirrors collect photons over $2 \times$ FWHM of the incident beam spatial distribution. The grazing angle for the KB mirror has been set at $\theta = 14$ mrad, by taking account of available space in the existing tunnel and hutch. For the heat load on the KB mirror, we consider only the fundamental of the FEL beam, as spontaneous emission and FEL higher harmonics are mostly removed by the flat distribution mirrors located upstream. The divergence of the FEL beam fundamental decreases as the photon energy increases. The shape of the beam, viewed in a cross section perpendicular to the propagation direction, is a solid circular spot. The useful projected beam footprint length on the mirror is defined as $L_{\text{footprint}} = 4.7\sigma$, which corresponds to $2 \times$ FWHM, and is depicted in Fig. 1, together with the beam divergence, as a function of the beam photon energy. The beam footprint length shown in Fig. 1 is calculated by using the effective distance between the KB mirror system and the source point in the undulator line. The flat distribution mirrors and KB mirrors could simply be polished silicon blocks, without an additional deposited coating, or could have an SiB_3 coating, which is now under investigation. The reflectivity of each of these mirrors is between 0.86 and 0.92 in the required photon energy range

---

[1] We use the term 'top-up-sides' to indicate the location on the mirror substrate to which cooling is applied. Consider the mirror in an orientation with the polished surface facing up. The substrate edge sides, adjacent to the polished surface, are of two types: long sides, whose long edges are roughly parallel to the incident beam direction, and short sides, whose widths are perpendicular to the incident beam. Cooling is applied to the upper portions of the long sides, just adjacent to the polished top surface, *i.e.* top-up-sides. See Fig. 2(*a*) for the case of a vertical deflecting mirror.
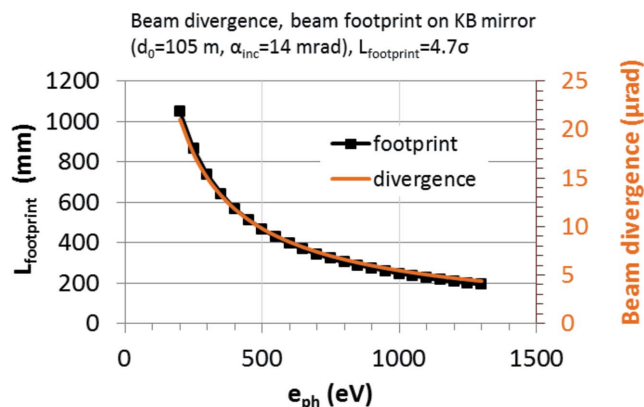
Figure 1
Beam divergence (orange line, right axis) and useful beam footprint length (black line, left axis) on the KB mirror, as a function of the FEL fundamental beam photon energy.

Figure 2
(*a*) 'Top-up-sides'-cooled mirror for vertical beam deflection: silicon substrate + two intermediate silicon blocks (on both sides) + two copper cooling tubes. Finite-element model (one quarter of the mirror) with (*b*) Gaussian power distributed heat load and (*c*) cooling boundary conditions.

(200–1300 eV). For a 20 W FEL photon beam power upstream of the first flat mirror, the absorbed power by the KB mirrors is up to 2 W. We will assume a 2 W heat load on the mirror in subsequent sections, unless otherwise indicated. To minimize the thermal distortion of the KB mirror, we first neglect the mirror bending requirement, to accommodate multiple focus locations and consider a mirror of rectangular shape. This mirror geometry is similar to the flat distribution mirrors for LCLS-II and to white beam mirrors for synchrotron beamlines. Therefore, the results below should also be valid for such mirrors. The mirror length chosen is 1000 mm; the useful polished optic length can reach 900 mm. This is long enough to provide 2 × FWHM beam collection above 250 eV and 1.7 × FWHM at 200 eV. Preliminary studies have been carried out to compare different indirect contact cooling schemes and different mirror cross sections. The results showed that top-up-sides cooling, with a cooling length shorter than the beam footprint, gave smaller mirror thermal deformation. From this preliminary study, and consideration of the mirror bending requirement, we adopted a mirror cross section of 20 mm height and 60 mm width. The final, bendable KB mirror will utilize the results of this study for thermal deformation minimization, but is not the subject of this paper.

2.2. Finite-element model of the mirror

The silicon mirror substrate is cooled by contact with two blocks (Fig. 2*a*). Eutectic Ga–In is used in the mirror contact interfaces to minimize the mechanical constraint effects of the cooling blocks. The water-cooling blocks consist of copper cooling tubes coupled to a silicon intermediate block with a thin interface layer of Ga–In eutectic liquid or an indium foil. The mirror substrate is 1000 mm long, 60 mm wide and 20 mm thick. The cross section of the silicon intermediate block is 20 mm wide and 10 mm thick. The copper cooling tube is 10 mm wide. Only a quarter of the mirror substrate, with the silicon intermediate block, is modelled, to take advantage of symmetry. The finite-element model (FEM), with Gaussian power distributed heat load and cooling boundary conditions,
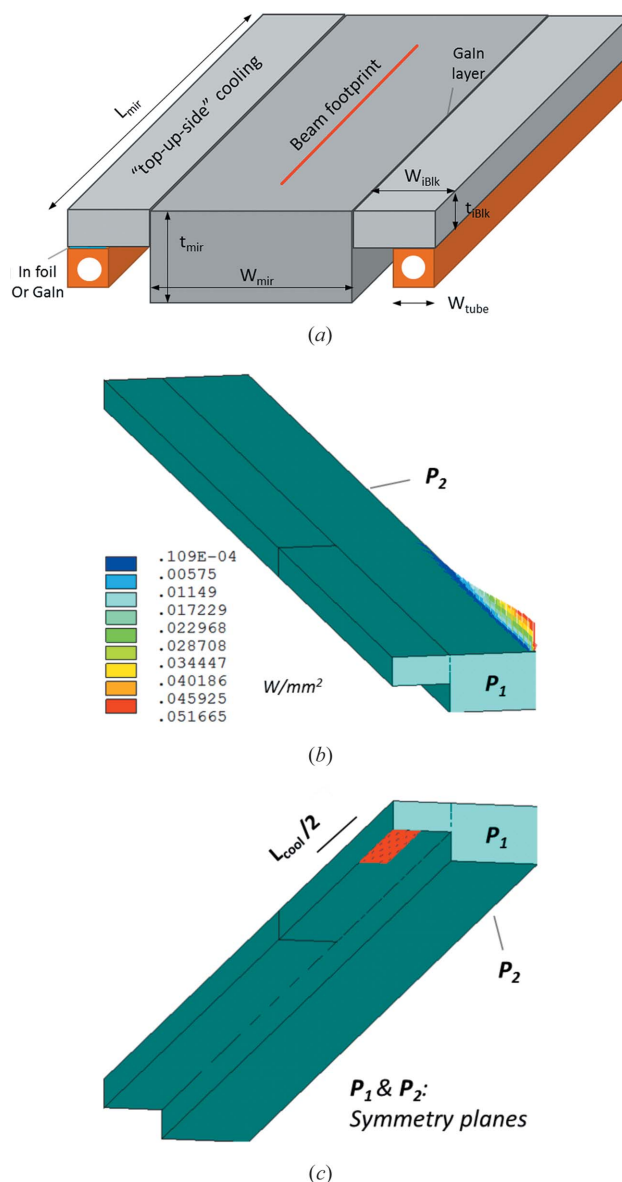
is illustrated in Figs. 2(*b*)–2(*c*). The contact interface between the mirror and the intermediate block is modelled in heat transfer with a thermal conductance of 0.1 W mm^{-2} °C^{-1}, thanks to the use of eutectic Ga–In (Khounsary *et al.*, 1997). For grazing incidence and the FEL photon energy range considered here, we can reasonably assume that the power is absorbed at the mirror surface. The total absorbed power is 2 W for 20 W of incident X-ray FEL (XFEL) beam power. The power density depends on the photon beam footprint size, or, equivalently, the FEL photon energy. The heat load is applied over a footprint length of 6σ, but we analyse the results of the mirror shape over a length $L_{\text{footprint}} = 4.7\sigma$. The copper cooling tubes are not represented in the model, as in previous studies

(Zhang, 1993; Zhang *et al.*, 2001, 2003, 2013*a*). Instead, an effective cooling coefficient of 0.005 W mm^{-2} $^{\circ}$C^{-1}, with a coolant temperature of 22°C, is applied to a cooling length L_{cool} on the silicon intermediate block (Fig. 2*c*) in the finite-element analysis (FEA). The length L_{cool} ($\leq$ length of the mirror L_{mir}) is a parameter to be optimized. As we are focusing on pure thermal deformation in this paper, we apply mechanical boundary conditions corresponding to a silicon substrate free of mechanical constraints.

The optical quality and performance of the mirrors can be quantified using the Strehl ratio (Strehl, 1902) which is expressed as

$$SR = \exp(-\varphi^2) \tag{1}$$

with

$$\varphi = \frac{4\pi\delta h \sin\theta}{\lambda}, \tag{2}$$

where φ is the phase error on the propagating beam of wavelength λ, incident at angle θ, due to the mirror optical surface shape error δh, an RMS height variation. The mirror shape error requirement can be expressed as:

$$\delta h\,[\text{nm}] = \frac{1240[-\ln(SR)]^{1/2}}{4\pi\sin\theta}\frac{1}{e_{ph}\,[\text{eV}]}. \tag{3}$$

LCLS-II requires a Strehl ratio of 0.97 for the stringent preservation of FEL wavefront and photon flux. The mirror shape error requirement for the KB mirrors (θ = 14 mrad) is as low as 1 nm, illustrated in Fig. 3, as function of photon energy.

To quantify the thermal deformation of the mirror for a given case, for instance, a given cooling length, we calculate an RMS residual height error as follows. First, we compute the displacement Uy normal to the mirror surface along the beam footprint centre, over a length $L_{footprint}$ = 4.7σ. Then a best spherical fit (BSF) is made, to obtain a function Uy_{fit}, because this spherical fit can be corrected using the bender mechanism for the KB mirrors. Next, we subtract this BSF from the FEA results Uy, to calculate the residual height error as
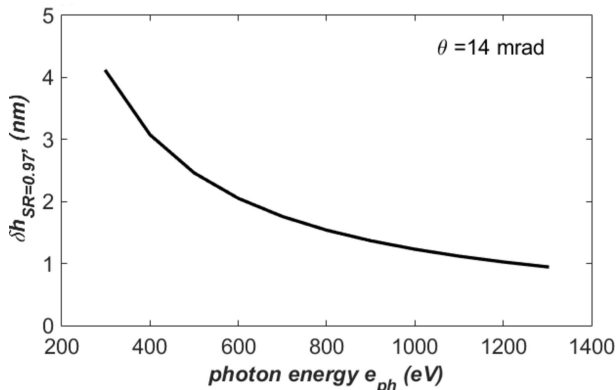

Figure 3
Mirror shape error requirement corresponding to a Strehl ratio = 0.97 and for the KB mirrors (θ = 14 mrad), *versus* photon energy.

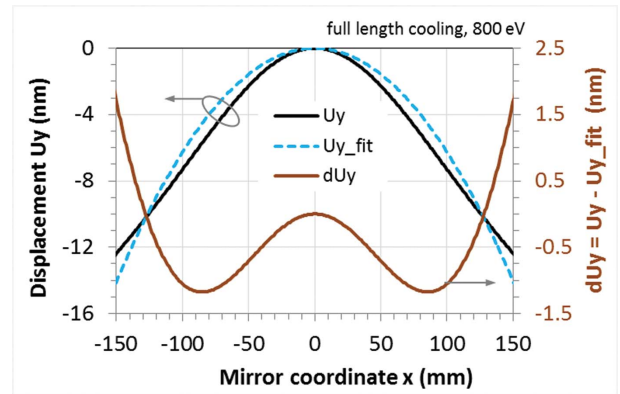**Figure 4**
Displacement normal to the mirror surface Uy (black line), best spherical fit (BSF) Uy_{fit} (dashed cyan line) and residual displacement dUy (brown line) along the beam footprint.

$$\mathrm{d}Uy = Uy - Uy_{fit}. \tag{4}$$

Finally, an RMS value of the residual height error RMS$_{dUy}$ is calculated. This value will be defined as the objective function in our optimization process, and the function to be minimized.

As an example, the displacement Uy, the BSF Uy_{fit} and the residual height error dUy along the footprint are depicted in Fig. 4, for a photon energy e_{ph} = 800 eV, with full-length cooling. The RMS value of the displacement Uy is 6.73 nm. After BSF subtraction, the RMS value of the residual height error RMS$_{dUy}$ is reduced to 0.84 nm. The radius of curvature of the BSF is R_{fit} = 800 km.

3. Top-up-side cooling with variable cooling length

3.1. General description

The pulsed FEL photon beam heats the mirror and this leads to a spatially and temporally varying temperature distribution in the mirror. The time-dependent temperature is a saw-tooth function, which can be treated as a superposition of two components, which are related to an average power and power from a single pulse. The temporal effects of multiple pulses will be discussed in a separate paper. Here, we consider only the effects of absorbed average power – a steady-state analysis.

The temperature distribution in space depends on both the heat-load distribution and the cooling conditions. For the LCLS-II SXR mirrors, we optimize the cooling scheme and parameters to minimize the thermal deformation. In a previous study (Zhang *et al.*, 2012) and in a preliminary study for the LCLS-II KB mirrors, we identified that top-up-sides cooling is one of the most attractive cooling schemes. When the beam footprint is significantly shorter than the mirror length, we can choose to cool the mirror on the top-up-sides but with a cooling length shorter than the beam footprint length. This reduces temperature variation along the mirror centre, meridional axis and, consequently, the thermal bump effects. Xu *et al.* (2013) have compared two different side

cooling surface areas: (*a*) 250 mm full length and 10 mm height, (*b*) smaller cooling surface area 215 mm long and 6 mm height. With configuration (*b*), the thermal slope error is smaller in the meridional direction, and only a few percent larger in the sagittal direction. The two flat distribution mirrors for the LCLS-II SXR will be top-up-sides cooled, with a shorter cooled length than the mirror length, for the variable incident beam footprint (Srinivasan *et al.*, 2014).

In the following section, we address the following questions: (1) What is the optimal cooling length for any beam footprint? (2) What is the correlation between the optimal cooling length and the beam footprint? (3) How does this optimal cooling length depend on the effective cooling coefficient? (4) What is the performance of this cooling technique? (5) How sensitive is the performance to the accuracy of the cooled length?

3.2. Optimization results

In §2.2, we presented an FEM of the mirror and defined the residual height error RMS_{dUy} as the objective function. The ANSYS APDL (see ANSYS documentation) optimization module (/opt) is used for cooling length optimization under ANSYS 15.0[2]. The design variable is the cooling length L_{cool}, as shown in Fig. 2(*c*).

We have performed the optimization at different FEL beam photon energies, corresponding to different beam footprints. Plots of residual height error RMS_{dUy} *versus* cooling length L_{cool} are shown in Fig. 5 for photon energies between 300 eV and 1300 eV. These results clearly display a minimum for RMS_{dUy} for each given photon energy. The corresponding cooling length is the optimized length, $L_{cool-opt}$.

In practice, the effective cooling coefficient depends on the water flow rate in the cooling tube, and the thermal conductance between the cooling block and the silicon mirror substrate. The effective cooling coefficient can vary from 0.002 to 0.01 W mm^{-2} °C^{-1}, or even more. To be most generally applicable, the method of minimizing the thermal deformation by varying the cooling length should yield an optimized cooling length that is independent of the effective cooling coefficient. To test this point, we also carried out a similar optimization for two additional cooling coefficients: 0.002 and 0.01 W mm^{-2} °C^{-1}. The optimized cooling lengths *versus* photon energy are plotted in Fig. 6 for three values of effective cooling coefficient. Almost identical results demonstrate that the optimized cooling lengths are not sensitive to the cooling coefficient. We know that thermal deformation and thermal stress depend on the temperature gradient, but not on the absolute temperature, if the material properties do not change significantly within the temperature range. When the cooling coefficient varies around 0.005 W mm^{-2} °C^{-1}, the temperature in the mirror changes by essentially a uniform value (an offset) and the temperature gradient is significantly unchanged. The optimal cooling length (shown in Fig. 6) decreases from 331 to 32 mm as the photon energy is increased
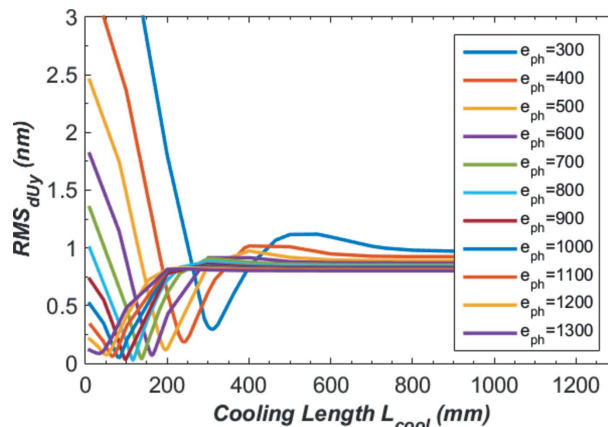
[2] Unfortunately, starting from ANSYS 14.0, optimization in APDL is no longer documented, and has become a legacy feature, but commands starting with OP still work in APDL.

Figure 5
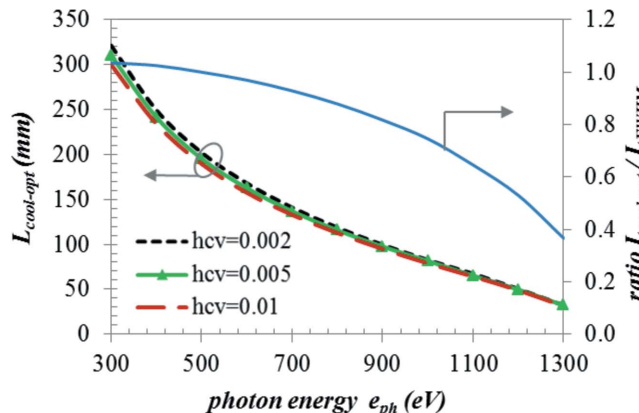Residual height error *versus* cooling length, at different photon energies.

Figure 6
Optimized cooling length *versus* photon energy for different cooling coefficients (left axis). Ratio between optimized cooling length and one FWHM beam footprint length (right axis).

from 300 to 1300 eV. Qualitatively, this is similar to the beam footprint length *versus* photon energy (Fig. 1). The ratio between this optimal cooling length and one FWHM beam footprint length is also depicted in Fig. 6. The value of the ratio varies from 1.04 at 300 eV to 0.37 at 1300 eV.

When an ideal beam with uniform power illuminates the entire mirror length (meridional axis), there is no temperature variation along that axis. But when the beam footprint is much shorter than the mirror length, thermal conduction in the meridional direction induces temperature variation in that direction. This creates a thermal bump component which is not spherical and cannot be corrected using a mechanical bender. But by using a cooling length shorter than the beam footprint length, we can reduce this thermal conduction and temperature variation in the meridional direction. This leads to a reduction in thermal deformation. Fig. 7 shows the temperature distribution of the water-cooled mirror with full-length and optimized-length ($L_{cool-opt} = 32$ mm) cooling, for the case of $e_{ph} = 1300$ eV, but with 20 W of absorbed power. With optimized cooling length, which is much shorter than the beam footprint ($L_{cool-opt}/L_{FWHM} = 0.37$ for the 1300 eV case),
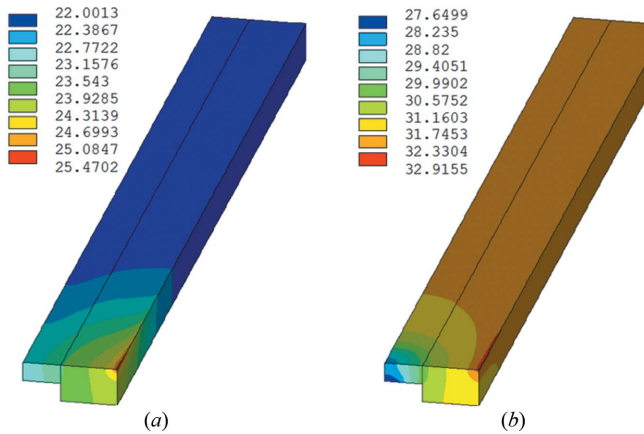
Figure 7
Temperature distribution (°C) with (a) full-length and (b) optimized-length cooling, at 1300 eV.

the temperature along the beam footprint is more uniform than in the case with full-length cooling. More uniform temperature distribution in the mirror leads to smaller thermal deformation.
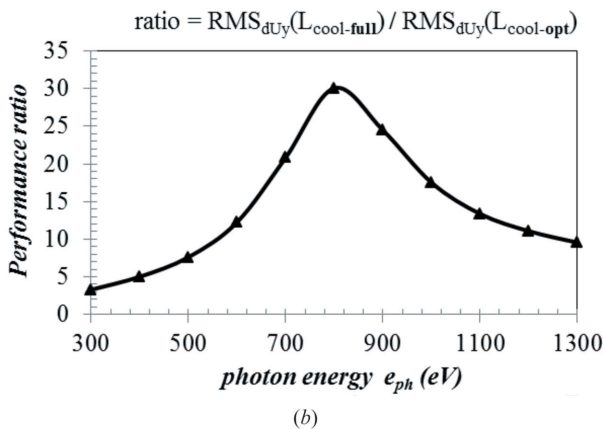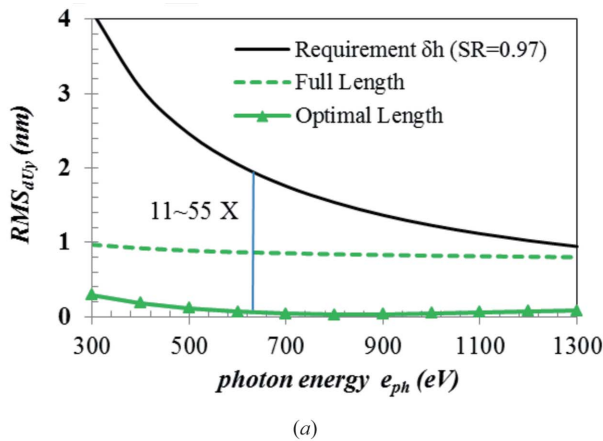

Figure 8
(a) Residual height error RMS_{dUy} with the optimal cooling length (green line), with full-length mirror cooling (dashed green line), and the residual height error requirement δh corresponding to a Strehl ratio = 0.97 (black line). (b) Performance ratio between RMS_{dUy} calculated with $L_{cool-full}$ and $L_{cool-opt}$ *versus* photon energy.

We can evaluate the performance of this cooling technique by comparing the minimized residual height error RMS_{dUy} (green line, Fig. 8a) with either the residual height error corresponding to a full-length-cooled mirror (dashed green line, Fig. 8a) or the residual height error requirement δh corresponding to a Strehl ratio = 0.97 (black line, Fig. 8a). The residual height error RMS_{dUy} can be minimized to 0.03 nm at 800 eV. Compared with full-length cooling, the residual height error RMS_{dUy} can be significantly reduced using optimized short-length cooling [Fig. 8b: performance ratio of RMS_{dUy} calculated with $L_{cool-full}$ and $L_{cool-opt}$, *i.e.* performance ratio = $RMS_{dUy}(L_{cool-full})/RMS_{dUy}(L_{cool-opt})$]. The reduction factor reaches 30 at 800 eV. The performance ratio drops to 3.3 at 300 eV. For 20 W XFEL beam power, the residual height error with full-length cooling is below the requirement for the considered photon energy range. The minimized residual height error RMS_{dUy} is about 11–55 times smaller than the required residual height error δh. The thermal deformation is proportional to the absorbed power. If the absorbed power is increased by a factor of 10, *i.e.* the average incident XFEL beam power is 200 W, the thermal deformation in terms of residual height error is still below the requirement when using optimized-length cooling. But the deformation of the full-length-cooled mirror exceeds the requirement. Therefore, variable-length cooling could be used to satisfy the mirror performance requirement for 200 W of XFEL beam power.

Optimized cooling length, shorter than the beam footprint, leads to a more uniform temperature distribution in the mirror and reduces the thermal deformation compared with full-length cooling. Is it possible to use a single shorter-length cooling block to reduce the thermal deformation over the entire photon energy range? This is an attractive question because a single cooling block is easier to implement than variable-length cooling. To answer this question, we have simulated the mirror with a single-length cooling block for all photon energies, for various values of length L_{cool} = 100, 200, 300, 500, 1000 mm. The results on residual height error RMS_{dUy} are depicted in Fig. 9. With one single, shorter-length

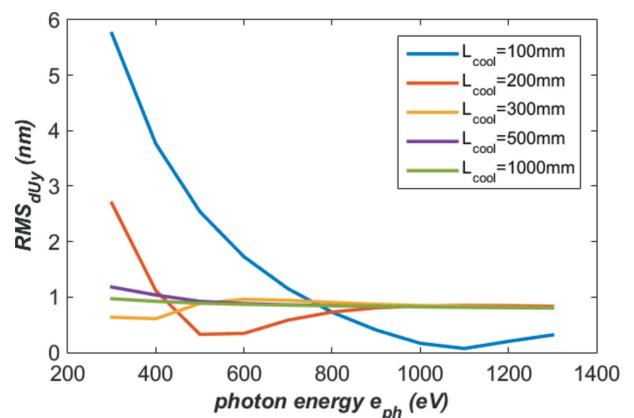**Figure 9**
Residual height error RMS_{dUy} for a single-length (L_{cool}) cooled mirror for all photon energies, for various values of the length L_{cool} = 100, 200, 300, 500, 1000 mm.
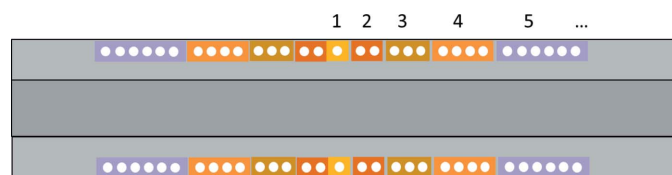
Figure 10
Hydraulic cooling tube arrangement for a variable-length-cooled mirror (back face view).

Figure 11
Schematic diagram of a mirror with electric heaters of adjustable length: (a) cross section, (b) top view.

cooling block, it is possible to significantly reduce the thermal deformation over a small photon energy range, for instance with L_{cool} = 100 mm, but the deformation increases significantly in the rest of the photon energy range. A single cooling length, if above 400 mm, gives quite uniform performance over the whole photon energy range.

In summary, a single-length-cooled mirror can meet the thermal deformation requirements for the case of 20 W average incident XFEL power. Variable-length cooling is needed to meet the thermal deformation requirements in the case of 200 W average XFEL power.

3.3. Implementation considerations

For N given cases of beam footprint length, it is possible to design a cooling system with $M \leq N$ independent hydraulic circuits. Each circuit is remotely controlled with a hydraulic valve. Fig. 10 illustrates a mirror with M independent cooling circuits ($M = 5$) and $4M - 2$ cooling blocks. Blocks with the same colour are connected in series to form one circuit and are each controlled by a single hydraulic valve. From the results shown in Fig. 5, we observe that a variation of ± 5 mm in the cooling length from $L_{cool-opt}$ does not significantly compromise the performance of the method. It is also possible to choose a block length to cover two footprint lengths close to each other for a slightly degraded performance. Of course, alternative designs exist for the cooling block implementation, for instance, using a trough in the mirror substrate with Ga–In eutectic liquid. In this case, a water cooling tube or blade is immersed in the eutectic Ga–In.

4. Full-length cooling with electric heater compensation

4.1. Design description

The method of using optimized variable cooling length, shorter than the beam footprint, is effective in minimizing thermal deformation. For variable beam footprint length, when changing photon energy, multiple cooling lengths are needed, as well as multiple hydraulic valves to switch on/off the water flow. In some circumstances, it might not be convenient to have multiple cooling blocks and multiple hydraulic valves. Therefore, we propose another method, based on a similar principle. We use a long, single cooling block on each side of the mirror, and add electric heaters between the cooling blocks and the mirror substrate, as illustrated in Fig. 11. There are four stripes of thin-film electric
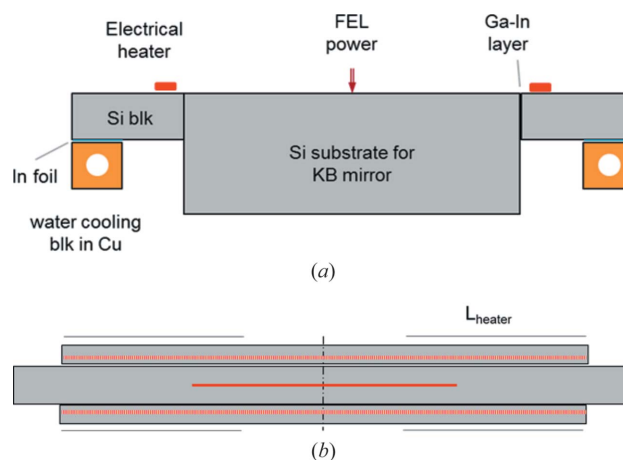
heaters, and each stripe consists of a number of cells along the mirror length. The total effective length of the electric heater can be adjusted using simple electric power supplies, i.e. energize only the heaters needed for a particular situation. Monitoring electric power supplies is easier and more cost-effective than monitoring cooling water flow. An electric heater, with a powered length L_{heater}, as shown in Fig. 11(b), overrides the cooling effects over this length. Consequently, the effective cooling length of the mirror is shortened. By optimizing the length and power of the heater, we can again minimize the thermal deformation of the mirror.

4.2. Modelling and optimization results

To simulate a mirror with cooling blocks and electric heaters, we apply symmetry boundary conditions and consider only a quarter of the mirror assembly. The intermediate silicon block is in contact with the mirror substrate, the cooling block and the electric heater. The contact interface between the mirror and the intermediate block is modelled in heat transfer with a thermal conductance of 0.1 W mm^{-2} °C^{-1}, thanks to the use of eutectic Ga–In (Khounsary et al., 1997). The cross section of the intermediate silicon block is 20 mm × 10 mm. The width of the cooling block is 10 mm. An effective cooling coefficient of 0.005 W mm^{-2} °C^{-1}, with a 'coolant temperature of 22°C', is applied to the 10 mm width on the intermediate Si block, over the whole length. The electric heater is 5 mm wide, with 1 mm clearance to the eutectic Ga-In interface. We neglect the mechanical effects of the intermediate block assembly on the mirror because we are focusing on a purely thermal deformation. Moreover, this mechanical effect is difficult to describe and model accurately. The FEM is shown in Fig. 12, with beam heat load and electric heating power boundary conditions.

As mentioned in §4.1, we have two parameters to optimize for a given footprint length/photon energy: the length L_{heater} and power density Pa_{heater} of the electric heater. When there are two or more design variables, ANSYS APDL optimization
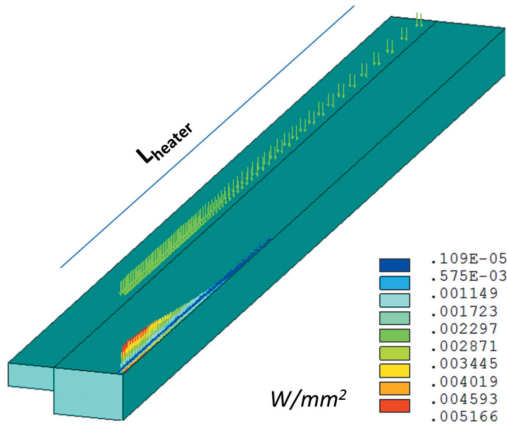
Figure 12
FEM of the mirror with beam heat load (800 eV, 2 W) and electric power heating. The length of the heater is L_{heater}.

modulus (/opt) is effective only when the design variables are limited to a small range. For a large range of design variables, the optimization often erroneously converges to some local minimum. Therefore, optimization of heater parameters is performed in two steps: (1) a preliminary optimization, with only one design variable L_{heater} (or Pa_{heater}) for a series of given values of the other parameter Pa_{heater} (or L_{heater}), (2) the results from the preliminary optimization allow definition of a small range of the two parameters (L_{heater} and Pa_{heater}); thus, we can refine the optimization with the two design variables (L_{heater} and Pa_{heater}). From the results for optimal cooling length, presented in §3, we can estimate the optimal heater length as

$$L_{\text{heater-opt}} \approx L_{\text{mir}}/2 - L_{\text{cool-opt}}/2. \qquad (5)$$

This facilitates the preliminary optimization (step 1). For example, at photon energy $e_{\text{ph}} = 800$ eV, $L_{\text{cool-opt}}$ is equal to 116 mm; therefore, $L_{\text{heater-opt}}$ is about 442 mm. The preliminary optimization for 800 eV can be carried out around this value, for example, $L_{\text{heater-opt}} = 420, \ldots, 460$ mm. Now,
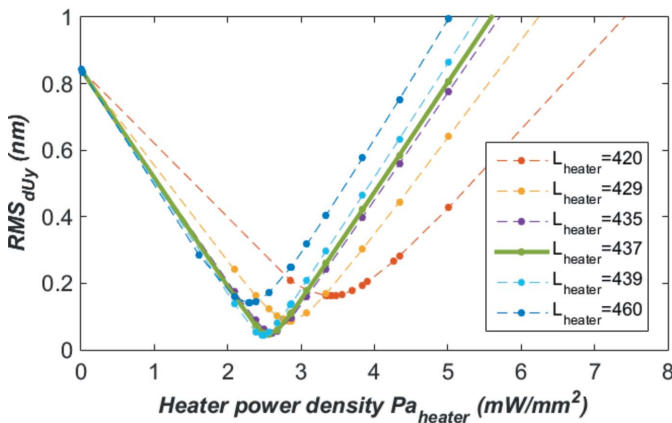
Table 1
Optimization results for full-length-cooled mirror with different cooling coefficients and beam power or mirror-absorbed power at $e_{\text{ph}} = 800$ eV.

P_{beam} is beam power, P_{abs} is mirror-absorbed power, h_{cv} is cooling coefficient, L_{heater} is heater length, Pa_{heater} is heater power density, $\text{RMS}_{\text{d}Uy}$ is residual height error and P_{heater} is total heater power. The bold entries show the varied quantity for that case.

P_{beam} (W)	P_{abs} (W)	h_{cv} (W mm^{-2} °C^{-1})	L_{heater} (mm)	Pa_{heater} (mW mm^{-2})	$\text{RMS}_{\text{d}Uy}$ (nm)	P_{heater} (W)
20	2	**0.005**	439	2.47	0.043	21.7
20	2	**0.002**	439	2.14	0.039	18.8
20	2	**0.01**	439	2.79	0.047	24.5
200	**20**	0.005	439	24.7	0.432	217
2000	**200**	0.005	439	247	4.32	2166

only heater power density Pa_{heater} is then a design variable. The residual RMS height error is plotted *versus* heater power density, for different values of the heater length, in Fig. 13. We observe an optimal heater power density for every heater length. The smallest value for $\text{RMS}_{\text{d}Uy}$ is 0.043 nm, with $L_{\text{heater-opt}} = 439$ mm and $Pa_{\text{heater}} = 2.47$ mW mm^{-2}. The final optimized heater length is about 0.7% higher than the one estimated by equation (4) for the case of $e_{\text{ph}} = 800$ eV.

To show the sensitivity of the minimized residual height error $\text{RMS}_{\text{d}Uy}$ to heater length and power density, we collect the minimum point of all the curves shown in Fig. 13, and depict the residual height error $\text{RMS}_{\text{d}Uy}$ and the corresponding heater power density *versus* the heater length in Fig. 14. These results clearly confirm the global optimization results for 800 eV, mentioned above. A ± 2 mm accuracy in heater length will not degrade the performance by as much as 7%. The electric heater power density can be easily monitored.

We have also performed analysis with different effective cooling coefficients ($h_{\text{cv}} = 0.005, 0.002, 0.01$ W mm^{-2} °C^{-1}) and different absorbed beam power ($P_{\text{beam}} = 2, 20, 200$ W). The optimization results (residual height error $\text{RMS}_{\text{d}Uy}$, heater length L_{heater} and power density Pa_{heater}) are given in Table 1. The optimized heater length L_{heater} is unchanged in all

Figure 13
Residual height error *versus* heater power density, for different heater lengths, for the case of photon energy = 800 eV.
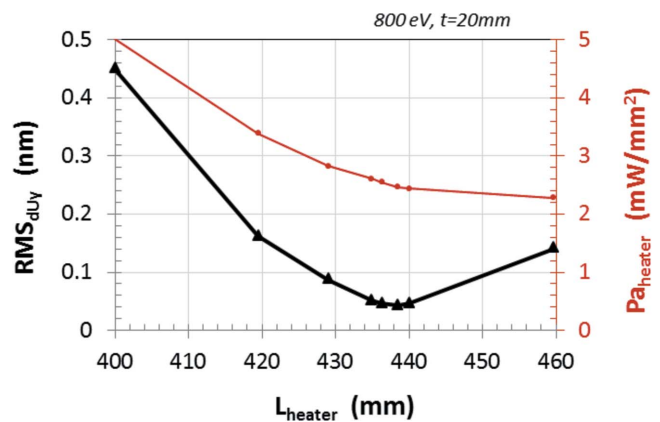

Figure 14
Residual height error $\text{RMS}_{\text{d}Uy}$ (left axis, black line) and the corresponding heater power density (right axis, red dashed line) *versus* heater length.

the cases. When increasing the effective cooling coefficient, the heater power density Pa_{heater} and the residual height error RMS_{dUy} increase slightly. The heater power density and thermal deformation (RMS_{dUy}) increase proportionally with absorbed power, when constant thermal conductivity and thermal expansion coefficients are used in the simulation. The total power generated by the electric heaters for the whole mirror, P_{heater}, can be calculated as

$$P_{heater} = 0.02\, L_{heater} Pa_{heater}. \qquad (6)$$

Results are given in Table 1 for e_{ph} at 800 eV. For 200 W of average incident XFEL power, the total electric heater power is 217 W. It is also possible to use a short cooling block, down to 400 mm, as discussed at the end of §3.2. We have made an additional heater optimization with a cooling block 500 mm long. The performance (residual height error) is identical to the case with a full-length cooling block above 500 eV and slightly different at lower photon energy (see Fig. 15a). The optimized heater length and power density at 800 eV are

188 mm and 2.48 mW mm^{-2}, respectively. The total electric heater power is then 93 W, compared with 217 W for the full-length cooling block.

It is very interesting and important to confirm that the optimal heater length is independent of the effective cooling coefficient and beam power.

Optimization of the electric heater parameters was extended to the entire photon energy range (300–1300 eV), and carried out for a 1000 mm-long cooling block (1 m C-Blk) and a 500 mm-long cooling block (0.5 m C-Blk). The minimized residual height error RMS_{dUy} (dashed-yellow and green lines in Fig. 15a) can be compared with the cases without heaters, and with full-length cooling (dashed black line in Fig. 15a) or without heaters but with optimized length cooling [solid black line in Fig. 15(a), as well as green line in Fig. 8(a)]. The residual height error RMS_{dUy} can be minimized to 0.02 nm by using optimal heater parameters (length and power density). Compared to the case without heaters, the residual height error RMS_{dUy} can be significantly reduced by up to a factor of 45 at 1300 eV. This technique, using electric heaters, leads to better performance (Fig. 15a) than the technique using variable-length cooling, especially at low and high photon energy. For instance, the residual height error RMS_{dUy} at 300 eV (1300 eV) is 0.13 (0.018) nm using optimized electric heaters, compared with 0.30 (0.084) nm using variable cooling length. Optimized heater parameters (length and power density) are shown in Fig. 15(b) and correspond to the residual height error RMS_{dUy} with optimal heaters in Fig. 15(a).

The optimal heater power densities are very close for the cases of 500 mm- or 1000 mm-long cooling blocks. The difference of the heater lengths between the two cases is about 250 mm. Using a 500 mm-long cooling block allows the reduction of total heater power by a factor of 2.2 at 1300 eV and by a factor of 3.0 at 300 eV. The total electric heater power can be calculated from equation (5), with the data shown in Fig. 15(b). For 200 W of XFEL beam power, the total heater powers are between 27 W (at 300 eV) and 214 W (at 1300 eV), if we use a 500 mm-long cooling block with electric heaters.

For both 500 mm- and 1000 mm-long cooling blocks, the variable portion (maximum − minimum) of the heater length (Fig. 15b) is 93 mm. The length of the heater cell unit should be variable: small near the centre of the mirror, larger when far away from the centre of the mirror. Each stripe of heaters can be composed of 10 to 20 units (or channels). The length of the units varies from 2 mm to 20 mm, with a single, extra-long unit at the outer ends. For instance, this extra-long unit is 120 (365) mm for the 500 (1000) mm-long cooling block.

(a)

(b)

Figure 15
(a) The residual height error RMS_{dUy} calculated in four cases: (1) with optimized heaters and 1000 mm-long cooling block (green line, 1 m C-Blk), (2) with optimized heaters and 500 mm-long cooling block (dashed yellow line, 0.5 m C-Blk), (3) without heater and with full-length cooling (dashed black line), (4) without heaters and with optimized length cooling (solid black line). (b) Optimized heater length (solid black line, dashed black line, left axis) and heater power density (solid red line, dashed red line, right axis) *versus* photon energy.

4.3. Discussion

Initially, using electric heaters is a way to approach variable-length cooling. Both techniques can be used to minimize the thermal deformation of a mirror for a given absorbed power distribution in steady state. They are not intended to make real-time correction on the timescale of the FEL pulses. We have already mentioned, at the beginning of §3.1, that we
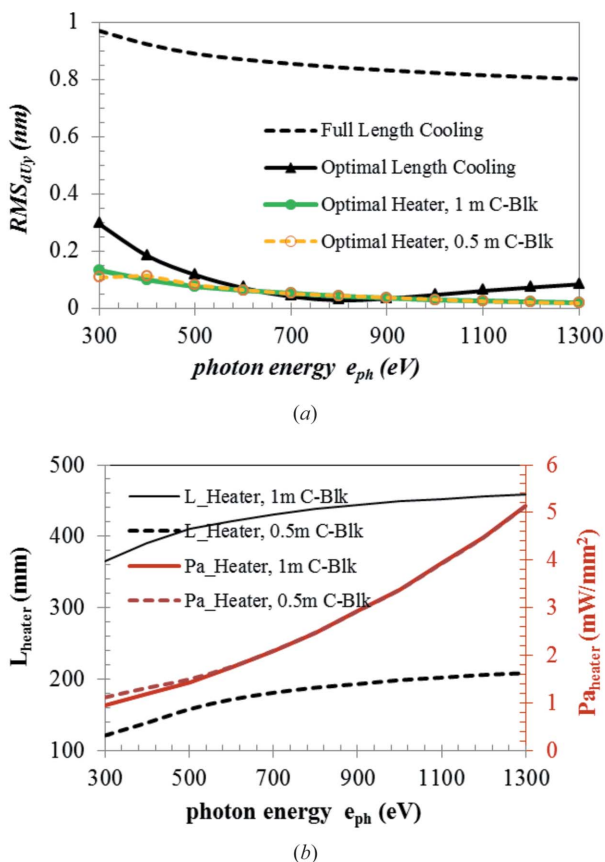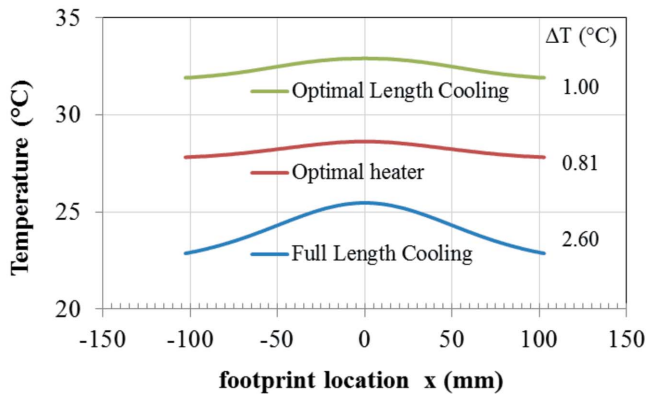
Figure 16
Temperature profile of the mirror along the footprint at $e_{ph} = 1300$ eV for mirror cases with: only full-length cooling (blue line), optimal heater + full-length cooling (red line), and optimal, variable-length cooling (green line). Results shown here are for 20 W absorbed power.

consider only the effects of the absorbed average power – a steady-state analysis.

We observe better performance with optimal heaters than with optimal-length cooling. This can be explained from the temperature distribution in the mirror. Fig. 16 shows the temperature profile of the mirror along the footprint at $e_{ph} = 1300$ eV, for the cases of (1) a mirror with only full-length cooling, (2) optimal heater + full-length cooling and (3) optimal, variable-length cooling. The cooling water temperature is assumed to be 20°C and mirror-absorbed power is 20 W (*i.e.* 200 W of incident XFEL power). The temperature level of the mirror with optimal heaters is higher than with only full-length cooling because of the additional heater power. At $e_{ph} = 1300$ eV, the cooling length in the case of optimal, variable-length cooling is only 32 mm (see Fig. 6), much shorter than the mirror length. The much smaller cooling surface area explains why the temperature with optimal, variable-length cooling is higher than with optimal heaters. The temperature variation within the footprint (ΔT) is 2.60°C with only full-length cooling, 0.81°C with optimal heaters + full-length cooling, 1.00°C with optimal, variable-length cooling. The thermal deformation of the mirror in terms of the residual height error is, qualitatively, related to this temperature difference. The technique of using electric heaters, combined with single-length cooling, leads to smaller temperature variation within the footprint and smaller thermal deformation than the technique of variable-length cooling. The fundamental reason is that we have two adjustable parameters to modify the temperature distribution with electric heaters (length and power density) and only one parameter for variable-length cooling (length).

The optimization of both electric heater and variable-length cooling is made for discretized photon energies of 300, 400, ..., 1300 eV. Between any two adjacent photon energies, the technique using electric heaters gives the possibility to optimize the heater power density and better smooth the performance for the whole photon energy range than the technique of variable-length cooling.

In §3.2, we have mentioned that variable-length cooling could be used to satisfy the LCLS-II KB mirror performance requirement for 200 W of XFEL beam power. The technique combining electric heaters and single-length cooling improves the performance. In the case using electric heaters, the tolerance requirement for heater power is easily achievable: ±10% of nominal (optimized) power at 1300 eV, ±17% at 800 eV and much more relaxed at 300 eV.

Note that the radius of curvature of the BSF is in the range of 1036 to 6567 km with variable-length cooling and 1107 to 4919 km with electric heaters. Indeed, the residual height error, in RMS, presented in this paper, is calculated after subtraction of this BSF. As the values of the radius of curvature are so large, and we also systematically compare the results of the two proposed techniques with full-length cooling, subtraction of the BSF does not alter the performance comparison of these two techniques.

4.4. Thermal slope minimization

In the previous sections, we presented two techniques for minimizing thermal deformation. The objective function was the residual height error, as explained in §2.2. To show the versatility of these methods, we also performed a design optimization minimizing the thermal slope error with the technique using variable cooling length. We now consider two different cross sections for the mirror: width 60 mm, thickness 20 or 60 mm. The objective function is the mirror RMS thermal slope error over the beam footprint length: RMS_{slope}, without subtraction of the best spherical fit.

RMS slope error results are depicted *versus* photon energy in Fig. 17, for mirrors 20 or 60 mm thick, with optimal-length or full-length cooling. The ratio of footprint length to mirror length is also plotted in Fig. 17 (blue line, right axis). With full-length cooling, the RMS_{slope} results are quite similar for thicknesses 20 and 60 mm, especially at photon energy above 800 eV. But the technique using variable cooling length leads to significantly better performance for the thick mirror
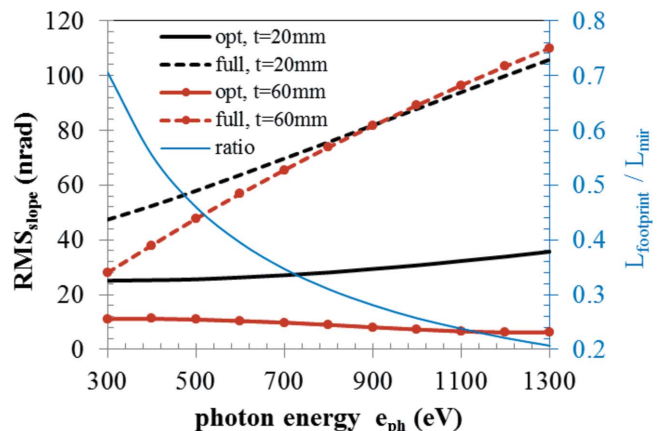

Figure 17
RMS slope error RMS_{slope} *versus* photon energy for mirrors 20 and 60 mm thick, with optimal-length and full-length cooling (left axis), and the ratio of the footprint length to mirror length (blue line, right axis).

(60 mm) than the thin mirror (20 mm). For the 20 mm-thick mirror, the thermal slope error with variable cooling length is reduced by a factor of between 1.7 and 3.0, compared with full-length cooling. For the 60 mm-thick mirror, this slope error reduction factor goes up to 17.5 at a photon energy of 1300 eV. The smallest slope error (6.3 nrad) at 1300 eV corresponds to a value of 0.2 for the ratio of beam footprint length to mirror length. The absorbed power is 2 W, as mentioned in §2.1. For an X-ray beam mirror under 300 W absorbed power (typical absorbed power for a white beam mirror in a high-energy third-generation synchrotron radiation beamline), the thermal deformation can, thus, be reduced to less than 1 µrad. There is still room for performance improvement by optimizing the mirror geometry to include notches.

5. Summary and conclusions

The thermal deformation of water-cooled X-ray mirrors under variable beam footprint is challenging, especially when the footprint is shorter than the mirror length. In this case, thermal conduction induces a temperature variation in the mirror meridional direction and creates a thermal bump component that is not spherical and cannot be corrected using a mechanical bender. To reduce the thermal conduction in this direction, as well as the thermal deformation, we proposed a technique using top-up-sides water cooling, with a shorter cooled length than the beam footprint length. The cooling length can be optimized. For the LCLS-II KB mirror, thermal deformation can be reduced by a factor of up to 30, compared with full-length cooling. Furthermore, we propose another alternative technique based on a similar principle; we use a long, single-length cooling block on each side of the mirror, and add electric heaters between the cooling blocks and the mirror substrate. The electric heaters consist of a number of cells along the mirror length. The total effective length of the electric heater can be adjusted using simple electric power supplies. The residual height error RMS_{dU_y} can be minimized to 0.02 nm by using optimal heater parameters (length and power density). Compared with the case of full-length cooling without heaters, the residual height error RMS_{dU_y} can be reduced by a factor of up to 45. The residual height error of the LCLS-II KB mirror, due to FEL heat load, can be reduced to 31–53 times smaller than the required residual height error δh. This means that, by using electric heaters, we can meet the thermal deformation limit for the KB mirror for an average XFEL incident power of 620 W.

The techniques presented here are also effective in reducing thermal slope errors. This opens their application to white beam mirrors in synchrotron radiation beamlines. For example, using the technique with optimized cooling length shorter than the beam footprint length, the RMS thermal slope error of a 1 m-long mirror can be limited to less than 1 µrad for 300 W absorbed power.

The technique using electric heaters with a single-length cooling leads to better performance than the technique using variable-length cooling, and offers more flexibility in mini-mizing thermal deformation when continuously tuning the photon energy. The length and the power density of the electric heater can be monitored and optimized. The optimization results presented in §4 are obtained with uniform power density in the heaters and the geometry shown in Fig. 11. The geometry of the mirror, the intermediate cooling block and electric heater assembly might be further optimized. By applying non-uniformly distributed power density along the mirror length, the optimization could be pushed further, to improve the performance beyond that presented in this study.

References

Amann, J. et al. (2012). Nat. Photon. **6**, 693–698.
Bilderback, D. H., Freund, A. K., Knapp, G. S. & Mills, D. M. (2000). J. Synchrotron Rad. **7**, 53–60.
Chapman, H. N. et al. (2011). Nature (London), **470**, 73–77.
Cocco, D. et al. (2013). Proc. SPIE, **8849**, 88490A.
Feldhaus, J., Saldin, E. L., Schneider, J. R., Schneidmiller, E. A. & Yurkov, M. V. (1997). Opt. Commun. **140**, 341–352.
Galayda, J. N. (2014). Proceedings of the 5th International Particle Accelerator Conference (IPAC'14), 15–20 June 2014, Dresden, Germany.
Khounsary, A. M. (1999). Proc. SPIE, **3773**, 78–87.
Khounsary, A. M., Chojnowski, D., Assoufid, A. & Worek, W. M. (1997). Proc. SPIE, **3151**, 45–51.
LCLS-II (2013). LCLS-II Conceptual Design Report. Technical Report. LCLS, Stanford, CA, USA.
Lee, W.-K., Fernandez, P. & Mills, D. M. (2000). J. Synchrotron Rad. **7**, 12–17.
Lee, W.-K., Fezzaa, K., Fernandez, P., Tajiri, G. & Mills, D. M. (2001). J. Synchrotron Rad. **8**, 22–25.
Lee, W. K., Mills, D. M., Assoufid, L., Blasdell, R. C., Fernandez, P. B., Rogers, C. S. & Smither, R. K. (1995). Opt. Eng. **34**, 418–425.
Mankowsky, R. et al. (2014). Nature (London), **516**, 71–73.
Marot, G., Rossat, M., Freund, A., Joksch, S., Kawata, H., Zhang, L., Ziegler, E., Berman, L., Chapman, D., Hastings, J. B. & Iarocci, M. (1992). Rev. Sci. Instrum. **63**, 477–480.
Mochizuki, T., Kohmura, Y., Awaji, A., Suzuki, Y., Baron, A., Tamasaku, K., Yabashi, M., Yamazaki, H. & Ishikawa, T. (2001). Nucl. Instrum. Methods Phys. Res. A, **467–468**, 647–649.
Ratner, D. et al. (2015). Phys. Rev. Lett. **114**, 054801.
Rogers, C. S., Mills, D. M., Lee, W. K., Knapp, G. S., Holmberg, J., Freund, A., Wulff, M., Rossat, M., Hanfland, M. & Yamaoka, H. (1995). Rev. Sci. Instrum. **66**, 2494–2499.
Seibert, M. M. et al. (2011). Nature (London), **470**, 78–81.
Srinivasan, V., Cocco, D., Krzywinski, J. & Kelez, N. (2014). 8th International Conference on Mechanical Engineering Design of Synchrotron Radiation Equipment and Instrumentation (MEDSI2014), 20–24 October 2014, Melbourne, Victoria, Australia.
Strehl, K. (1902). Z. Instrum. **22**, 213–217.
Xu, Z., Wang, N.-X., Li, Z., Song, L., Luo, H. & Wang, J. (2013). J. Phys. Conf. Ser. **425**, 052011.
Zhang, L. (1993). Proc. SPIE, **1997**, 223–235.
Zhang, L. (2010). Cutting-Edge Mirror Systems for ESRF Beamlines – White Beam Mirror Optimization. ESRF internal document: ISDD Day, 29 March 2010. ESRF, Grenoble, France.
Zhang, L., Barrett, R., Friedrich, K., Glatzel, P., Mairs, T., Marion, P., Monaco, G., Morawe, C. & Weng, T. (2013b). J. Phys. Conf. Ser. **425**, 052029.
Zhang, L. et al. (2012). 7th International Conference on Mechanical Engineering Design of Synchrotron Radiation Equipment and

Instrumentation (MEDSI2012), 15–19 October 2012, Shanghai, People's Republic of China.

Zhang, L., Hoszowska, J., Migliore, J. S., Mocella, V., Ferrero, C. & Freund, A. (2001). *Nucl. Instrum. Methods Phys. Res. A*, **467–468**, 409–413.

Zhang, L., Lee, W.-K., Wulff, M. & Eybert, L. (2003). *J. Synchrotron Rad.* **10**, 313–319.

Zhang, L., Sánchez del Río, M., Monaco, G., Detlefs, C., Roth, T., Chumakov, A. I. & Glatzel, P. (2013a). *J. Synchrotron Rad.* **20**, 567–580.